18th International Conference on Space Operations, Montreal, Canada, 26 - 30 May 2025.

SpaceOps-2025, ID # 529

Advancing Sustainability in Space Operations: Optimizing Laser Technologies for Enhanced Energy Transmission in the New Space Era

Ilyes Ghedjatti[a]*, Shiwei Yuan[a], Nan Yan[b], Haixing Wang[a]

[a] *School of Astronautics, Beijing University of Aeronautics and Astronautics, China, ilyes.ghedjatti@buaa.edu.cn*
[b] *School of Mechanical and Electrical Engineering, Beijing Institute of Technology, China*
* Corresponding Author

Abstract

The rapid evolution of space operations in the New Space era necessitates a comprehensive approach to sustainability, particularly in the development and application of advanced laser systems. This research addressed the pressing need for effective laser technologies capable of optimizing energy transmission in aerospace applications. By establishing dynamic optical configurations and an independent variables-based system, designed to optimize energy management over adjustable working distances, this study enhanced the laser-target interactions across various applications. These applications may encompass energy harvesting and transmission, telecommunications, energetic materials ignition, and energy-directed weapon systems deployment. In this research, to investigate the optimization of laser energy transfer and interaction, Boron Potassium Nitrate (BPN) was selected due to its high-performance, substantial combustion heat, robust ignition capability, inherent safety, and insensitive characteristics, making it a preferred choice in conventional weaponry and aerospace pyrotechnics. For this purpose, a BPN laser ignition experimental platform was developed, integrating a 2W 808-nm laser diode system, along with collimating lenses, a reverse-mode beam expander, and converging achromatic doublets, allowing for precise control over BPN ignition dynamics. The findings showed that the laser ignition optical path played a crucial role in determining ignition performance. For instance, experiments indicated that a 0% beam inverted magnification at a 75-mm ignition distance produced an equivalent BPN ignition delay time of 20 ms as observed with a 100% beam inverted magnification at a distance of 170 mm. This result underscored the significance of laser beam energy density in achieving effective ignition. The implementation of adjustable optical configurations enabled the simultaneous control of BPN ignition across varying conditions while optimizing energy requirements. The substantive merit of this research lies in its realistic approach to overcoming existing limitations in laser technology. The findings not only provide a robust framework for energy transmission but also align with the broader goals of enhancing operational efficiency and reducing costs in space missions. By addressing discrepancies noted in the current literature, this study reconciles converging and diverging hypotheses, thereby contributing to a more cohesive understanding of laser performance in aerospace contexts.

Keywords: Energy management, dynamic optical configurations, Boron Potassium Nitrate, laser ignition systems, laser-matter interactions.

Acronyms/Abbreviations

Boron Potassium Nitrate	BPN
International Organization for Standardization	ISO
Light-Emitting Diode	LED

1. Introduction

Laser technology has undergone significant advancements, expanding its applications across various fields. Industrial applications of lasers include additive manufacturing, cutting, welding, and material processing, where their precision and efficiency enhance productivity [1,2]. In scientific research, lasers play a pivotal role in spectroscopy, holography, and optical trapping, allowing for detailed analysis and manipulation of microscopic entities [3,4]. Furthermore, the field of communication heavily relies on lasers for fibre-optic systems, which enable high-speed data transmission over long distances [5]. Military applications also benefit from laser technology, including range-finding, target designation, and the development of directed-energy weapons [6]. An emerging application of lasers is in the ignition of energetic materials, such as explosives and propellants. Laser ignition of fuels and energetic materials presents several advantages over traditional ignition methods, including precise control over the ignition process, the capability for remote ignition, and the potential for miniaturization of ignition systems [7]. This technology is particularly advantageous in scenarios where reliability and safety are critical, such as in aerospace and defence [8].

To better understand the advantages and benefits laser systems can achieve, and to accurately determine the key optical and energy parameters through which optimal configurations can be implemented to achieve energy management, safety, and operational efficiency, Boron Potassium Nitrate was selected for laser ignition [9]. The aforementioned parameters are determined thanks to BPN's advantageous properties, including a high heat of reaction, substantial enthalpy, elevated combustion temperature, low molar mass, extended shelf life, thermal stability, and effective performance [10].

The methods of beam delivery and focusing are critical components in laser ignition systems. Traditional free-space beam delivery systems employ lenses and mirrors to focus the laser beam onto the target material. This approach typically involves beam expansion using an up collimator, beam direction adjustment via mirrors, and beam focusing through an objective lens. Alternatively, the laser power density on the target surface can be modified through two conventional means: by varying the power through voltage control in the electronic power pack regulating the current in a diode laser or by employing neutral density filters in the beam path. However, this latter technique faces challenges related to beam divergence over long distances and potential misalignment issues [11,12].

Unlike previous studies that encountered several obstacles in laser propagation leading to energy losses and decreased performance, the newly designed optical system overcame these limitations by conserving energy and minimizing losses even over larger working distances and effective focal lengths [13]. This was achieved by precisely controlling geometric (optical) parameters and energy-related metrics, enabling optimal laser-material interaction. In addition, the effect of varying effective focal lengths and working distances on the BPP was investigated, providing insights on the outcomes of manipulating and controlling the laser parameters, which offers more flexibility compared to fixed experimental setups used in other works [14,15].

2. Material and methods

The experimental setup design part contains two main sets of experiments conducted separately: (a) the first set covers the investigation of laser key parameters, laser beam propagation and manipulation, and the effect of laser parameters variation; (b) the second set covers the selection of the primary pyrotechnic for laser initiation, the selection process takes into consideration the material's military specifications (as shown in Table 1).

Table 1. BPN classification and properties

BPN Properties	**Detailed Description**	
Military specification	MIL-P-46994B(AR)	
Scope	This specification covers eight types of ignitor pellets/granules for use in rocket motors, fuzes, and payload ignition/expelling charges.	
Classification	Type I – Cylindrical	
Material composition requirements	Potassium nitrate	MIL-P-156 except particle size shall be 15 μm
	Boron, amorphous	MIL-B-51092 except particle size shall be ≤ 1.5 μm, and boron purity 90-92%
	Polyester resin	MIL-R-7575 Grade A, Class O, Form K
	Peroxide, methyl ethyl ketone	MIL-P-81351
Materials formulation	Potassium nitrate, %	70.7 ± 2.0
	Boron, amorphous, %	23.7 ± 2.0
	Binders, %	5.6 ± 0.5
Binder composition	Polyester resin, %	98.0 ± 1.0
	Catalyst, %	1.5 ± 0.1
	Accelerator, %	0.5 ± 0.01
Physical properties	Type	I-E – Cylindrical
	Diameter, mm	4
	Height, mm	5
	Minimum weight, gm	0.1
Physical and ballistic properties	Minimum density, gm/cm^3	N/A
	Max. moisture content, %	0.75
	Burning rate, mm/s	31.75 – 44.45
	Max. heat of reaction, cal/gm	1500
	Minimum crush strength, gm	5000 (Axial), 500 (Radial)

2.1 Experimental setup and protocols

The laser ignition platform (see Fig. 1) mainly consists of a 808 nm-laser system, optical devices to study and manipulate the beam propagation, measurement sensors to measure and record the variation of laser key parameters, as well as a computer for data processing and storage (as shown in Table 2). The experimental protocol aims to implement the main steps necessary for the dynamic configurations design and the study of the thermophysical properties, the governing heat transfer mechanisms, and the ignition dynamics and characteristics (see Fig. 2).

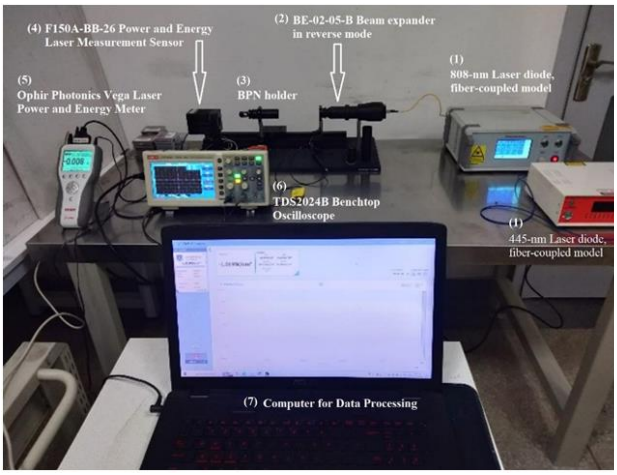

Fig. 1. Frontal view of the experimental setup

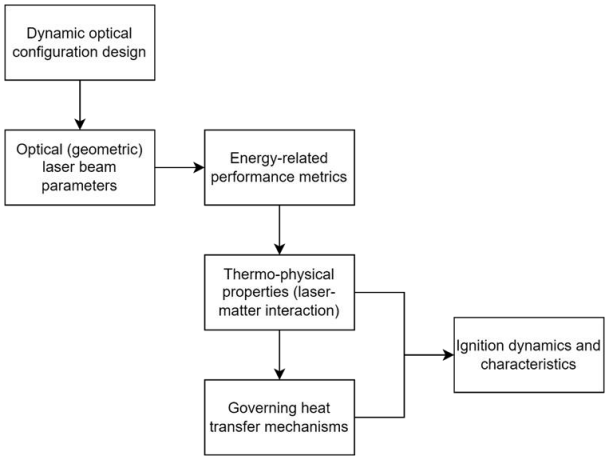

Fig. 2. Experimental protocol

Table 2. Experimental setup items and part numbers

Item	Part number
808-nm Laser diode, fiber-coupled model	DS3-21312-203
Collimating lens	C240 TMD-B
Beam expander	BE-02-05-B
Achromatic doublets	AC254-60-B-ML
	AC254-80-B-ML
	AC254-125-B-ML
N-BK7 Windows	WG31050-B
Photodiode	FDS1010
Benchtop oscilloscope	TDS2024B
Power and energy laser meas. sensor	F150A-BB-26
Laser power and energy meter	Ophir Photonics Vega
Thermocouple Smart Sensor	-
Electronic scale	-
Personal protection equipment	-

2.2 Optical system configurations and laser key parameters

The laser diode systems were used to set the desired variables such as wavelength (λ), input power (P_{input}), and pulse time (t_p). After that the beam radius ($\omega(z)$) and beam waist (ω_0) values were empirically defined, the energy-joule meter was used to measure the pulse energy (E_p), from these three parameters the laser intensity and brightness were estimated. During the measurements, the optical system configuration was continuously modified and different values of the inverted magnifying power (*iMP*) and compensator (*c*) of the beam expander in reverse mode were set, leading to a changing working distance ($d_{working}$) with the changes in *iMP* and *c*, at each focal length (f_{dblt}) of the selected achromatic doublets. The trials were carried out in the subsequent order: the fibre-coupled laser diode was employed to generate the laser signal, with a divergence angle of 12.6 degrees for the laser beam exiting the FC/PC fibre. The laser beam was then collimated using the collimating lens. Next, the collimated beam was transmitted to the beam expander used in reverse mode to decrease its diameter by different *iMP* levels. The output laser beam from the reverse-mode beam expander was focused using achromatic doublets with different f_{dblt}, targeting the power and energy laser measurement sensor.

By controlling the *iMP* of the reverse-mode beam expander, the working distance separating the achromatic doublets and the sensor was changed accordingly. Additionally, the compensator positions of the reverse-mode beam expander were varied over the range of 0-2 mm (with a capacity in the range of 0-7 mm), as this allowed to obtain different working distances and beam waists at the considered *iMP* and *c*, at each f_{dblt}. The sensor's positions were readjusted each time the *iMP* and *c* were modified so that the focal point would fall on the surface of the power-energy laser measurement sensor. A power- energy meter was used to display the measured data transmitted by the sensor. Finally, the displayed data was transferred to the computer for recording. At each trial, the controlled variables were the wavelength (λ = 808 nm), the compensator position (c = 0 mm and c = 2 mm), and the focal lengths of the achromatic doublets (f_{dblt} = 60 mm, f_{dblt} = 80 mm, and f_{dblt} = 125 mm).

The independent variables were the input power (from 0.5 W to 2 W, with a pace of 0.5 W), the pulse time (from 50 ms to 900 ms, with a pace of 50-100 ms), and the inverted magnifying power (1/2X, 1/3X, 1/4X, and 1/5X). The dependent variables covered the aspects of laser beam propagation through the optical system and free-space over the working distance (as shown in Table 3).

Table 3. Laser propagation- and manipulation-related main parameters

Variable classification	Variable nomenclature	Abbreviation	Unit
Controlled variables	Focal length of the achromatic doublet	f_{dblt}	mm
	Wavelength	λ	nm
	Compensator	c	mm
Independent variables	Inverted Magnifying Power	*iMP*	%
	Input power	P_{input}	W
	Pulse time	t_p	ms
Dependent variables	Beam radius	$\omega(z)$	mm
	Beam waist	ω_0	mm
	Working distance	z	mm
	Pulse energy	E_p	mJ
	Incident (average) intensity	I_a	W/cm^2
	Laser brightness	*Br*	W/sr.cm^2

2.3 Laser initiation of BPN

Conducted in an open-air environment, laser-BPN interaction, and the effect of laser parameters variation on the ignition characteristics of BPN were investigated. The laser diode systems were used to set the desired variables such as λ, P_{input}, and t_p. The $\omega(z)$, ω_0, E_p, I_a and *Br* were empirically defined. During the ignition trials, the optical system configuration was continuously modified and different values of the *iMP* and *c* of the beam expander in reverse mode were set, leading to a changing $d_{working}$ with the changes in *iMP* and *c*. The trials were carried out following the same protocol as for the previous set of experiments during the investigation on the optimal system configurations. However, this time, the output laser beam was focused in a way that the focal point falls on the surface of the BPN, which was placed within the BPN holder.

By controlling the iMP of the reverse-mode beam expander, the working distance separating the achromatic doublets and the BPN holder was changed accordingly. Additionally, the compensator positions of the reverse-mode beam expander were varied over the range of 0 2 mm. The positions of the BPN holder were readjusted each time the iMP and c were modified so that the focal point would fall on the surface of the BPN. The photodiode was placed between the protective window (protecting the achromatic doublet from the deflagration flyer) and the BPN holder to detect the first light emission related to the laser signal and the second light emission related to BPN initiation. The photodiode was then connected to the Benchtop oscilloscope in order to display and record the ignition delay time. The sensors connected to the thermocouple were placed inside the BPN holder on both surfaces of the BPN to record the maximum ignition temperature. Finally, all the measured data was transferred to the computer.

At each trial, the controlled variables were λ = 808 nm, c = 0 mm and c = 2 mm, and f_{dblt} = 60mm, f_{dblt} = 80mm, and f_{dblt} = 125mm. The independent variables were the input power, pulse time, and inverted magnifying power (1/2X, 1/3X, 1/4X, and 1/5X). The experimental configurations in terms of input power and pulse time were set according to the minimum input power and shorter pulse time required by the system so ignition can occur. The dependent variables covered the aspects of laser beam propagation through the optical system, free-space over the working distance, and the ignition characteristics (as shown in Table 4).

Table 4. BPN ignition-related main parameters

Variable classification	Variable nomenclature	Abbreviation	Unit
Controlled variables	Focal length of the achromatic doublet	f_{dblt}	mm
	Wavelength	λ	nm
	Compensator	c	mm
Independent variables	Inverted Magnifying Power	iMP	%
	Input power	P_{input}	W
	Pulse time	t_{p}	ms
Dependent variables	Beam waist	ω_0	mm
	Pulse energy	E_{p}	mJ
	Incident (average) intensity	I_{a}	W/cm^2
	Ignition delay time	t_{ign}	ms
	Ignition temperatures	T_{ign}	K

3. Theory and calculation

3.1 Laser beam characteristics and propagation

Gaussian irradiance profiles are symmetric around the beam's centre and decrease with increasing distance from the centre perpendicular to the direction of propagation [128-131]. Its irradiance I(r) is given by equation (1).

$$\mathrm{I}(r) = I_0 \exp\left(\frac{-2r^2}{\omega(z)^2}\right) = \frac{2P_{tot}}{\pi\omega(z)^2} \exp\left(\frac{-2r^2}{\omega(z)^2}\right) \tag{1}$$

Where I_0 is the peak irradiance at the beam's centre, r is the radial distance from the beam axis, $\omega(z)$ is the beam radius at which the irradiance falls to $1/e^2$ (13.5%) of I_0, z is the distance from the plane where the wavefront is flat, P_{tot} is the total power of the beam. In real cases, and with respect to beam propagation, changes need to be introduced due to lower beam quality, lower good focusability, and higher divergence at lower quality laser beams. The real laser beam is in relation to a theoretical best case that is the factor M^2, which is always larger than 1. The M^2 factor also determines the radiance of the beam. In addition to the M^2 factor, the Beam Parameter Product (*BPP*) is another metric used to evaluate the quality of a laser beam. It is defined as the product of the beam radius at the beam waist and the half-angle beam divergence. Since the *BPP* is directly proportional to the M^2 factor, a larger beam parameter product corresponds with a poorer quality beam. The minimum value of the *BPP* is λ/π and this can only occur for an ideal Gaussian beam. *BPP* is commonly used to characterize fibre or semiconductor lasers with large M^2 factors, as well as diode-laser fibre-coupled systems for determining the quantity of light that can be coupled into a fibre. Gaussian laser beams, including their beam radius, Rayleigh range, and BPP are defined by equations (2), (3), and (4); and by equations (5), (6), and (7) for real beams (as shown in Table 5).

Table 5. BPN ignition-related main parameters

Gaussian beam		Real beam	
$\omega(z)_{\text{Gauss}} = \omega_{0,\text{Gauss}} \sqrt{1 + \left(\frac{z}{z_{\text{R,Gauss}}}\right)^2}$	(2)	$\omega(z)_{\text{Real}} = \omega_{0,\text{Real}} \sqrt{1 + \left(\frac{z}{z_{\text{R,Real}}}\right)^2}$	(5)
$z_{\text{R,Gauss}} = \pi\, \omega_{0,\text{Gauss}}^2 / \lambda$	(3)	$z_{\text{R,Real}} = \frac{\pi\, \omega_{0,\text{Real}}^2}{\lambda\, M^2} = \frac{\pi\, \omega_{0,\text{Real}}^2\, K}{\lambda}$	(6)
$BPP_{\text{Gauss}} = \omega_{0,\text{Gauss}}\, \theta_{\text{Gauss}} = \lambda / \pi$	(4)	$BPP_{\text{Real}} = \omega_{0,\text{Real}} \cdot \theta_{\text{Real}} = \frac{\lambda M^2}{\pi} = \frac{\lambda}{\pi K}$	(7)

The beam quality factor M^2, or K, are both defined by equations (8) and (9).

$$M^2 = \frac{1}{K} = \frac{BPP_{\text{Real}}}{BPP_{\text{Gauss}}} = \frac{\omega_{0,\text{Real}}\theta_{\text{Real}}}{\omega_{0,\text{Gauss}}\theta_{\text{Gauss}}} > 1 \tag{8}$$

$$\omega_0 \cdot \theta = \lambda M^2/\pi = const. \tag{9}$$

Measuring M^2 is not as simple as measuring the beam profile at a single plane. ISO 11146 dictates that five beam radius measurements must be taken at different positions along the optical axis in both the near field and the far field.

It is possible to make a beam look like an ideal Gaussian at one specific plane without it containing any of the TEM_{00} mode at all. Even though the cross-section at that specific plane looks like a perfect Gaussian distribution, the beam will propagate very differently than a Gaussian beam with a greater divergence angle. Multiple radius measurements at different planes will quickly reveal the difference between this beam and a true Gaussian beam. The measured beam radius, $\omega(z)$, can be related to the beam waist (ω_0), the wavelength (λ), and the M^2 factor by equation (10).

$$\omega(z)^2 = \omega_0^2 \left[1 + (z - z_0)^2 \left(\frac{M^2\lambda}{\pi\omega_0^2}\right)^2\right] \tag{10}$$

One disadvantage of characterizing beams with the M^2 factor compared to other beam quality parameters is that it places more emphasis on the "wings", or lower-power density parts furthest away from the centre, making it suited for academic settings than industrial applications. The brightness of a light source is defined as the power emitted per unit surface area per unit solid angle. The maximum brightness is achieved for a perfectly spatially coherent laser beam. The brightness can be expressed by equations (11) and (12).

$$Br = P_{tot} / A\Omega \tag{11}$$

$$Br = P_{tot} / M^4\lambda^2 \tag{12}$$

Where P_{tot} is the laser power over the surface area A and Ω is the solid angle of divergence.

4. Results and discussion

4.1 Influence of iMP and c on the working distance, beam radius, and beam waist

The working distance increases from 70 mm to 170 mm as *iMP* increases from 0% to 100% for a 60 mm achromatic doublet at c = 2 mm, indicating significant adaptability in focusing capabilities (see Fig. 3). The beam radius increases from 6.25 mm to 8.46 mm with the increase in *iMP*, suggesting that as the working distance extends, the beam expands slightly at the level of the achromatic doublet. The beam waist exhibits an inverted U-shape, increasing from 0.125 mm to a maximum of 0.1875 mm at *iMP* = 66.66%, before decreasing back to 0.15 mm at higher *iMP* values. Both working distance and beam radius show a linear increasing trend with rising *iMP*, while beam waist demonstrates a non-linear behaviour characterized by its maximum point. The results indicate that adjusting *iMP* not only affects working distance and beam radius but also beam waist behaviour in a non-linear manner. The inverted U-shape of the beam waist suggests that there is an optimal range of magnification (~66.66% *iMP*) where the focusing capability is maximized before decreasing again. This behaviour indicates that beyond certain configurations, further increase in magnification may lead to suboptimal focusing conditions. The observed trends emphasize the need for careful consideration when designing optical systems for specific applications. Maintaining an optimal balance between working distance, beam radius, and waist is essential for achieving desired performance in laser ignition scenarios.

The working distance increases from 75 mm to 230 mm as *iMP* increases from 0% to 100% for a 60 mm achromatic doublet at c = 0 mm (see Fig. 4). The beam radius increases from 6.67 mm to 10.58 mm with the same increase in *iMP*, suggesting that as the working distance extends, the beam expands at the level of the achromatic doublet. The beam waist remains constant at 0.125 mm for *iMP* values between 0% and 33.33%, then increases to 0.1875 mm at *iMP* = 66.66%, and further to 0.2 mm at *iMP* = 100%. This indicates a non-linear behaviour in beam waist as *iMP* increases. Both working distance and beam radius exhibit a linear increasing trend with rising *iMP*, while beam waist demonstrates a more complex behaviour characterized by an initial flat region followed by an increase. The flat behaviour of the beam waist at lower *iMP* values suggests that there is an optimal range of magnification where focusing conditions are stable before transitioning to an increased focusing capability at higher magnifications. This behaviour indicates that adjustments beyond certain configurations may lead to improved focusing conditions but could also introduce complexities in managing beam quality.

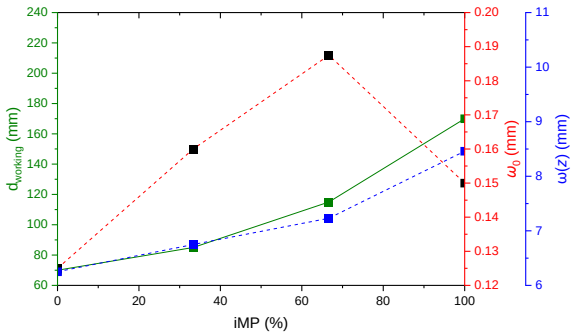

Fig. 3. Variation of $d_{working}$, ω_0 and ω(z) with *iMP* at c = 2 mm.

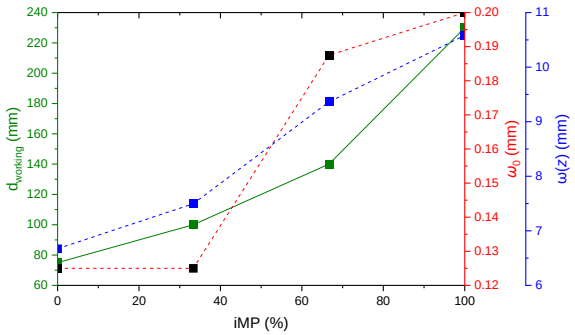

Fig. 4. Variation of $d_{working}$, ω_0 and ω(z) with *iMP* at c = 0 mm.

To compare the results from the two cases (c = 0 mm and c = 2 mm) with a 60 mm achromatic doublet, key observations were established. The working distance shows a greater range of adaptability in the case of c = 0 mm compared to when it is set at 2 mm. The beam radius increases more significantly in the case of c = 0 mm, indicating that the optical configuration allows for more expansion of the beam as it propagates. In both cases, the beam waist does not exhibit a linear relationship with *iMP*; however, it behaves differently between the two configurations. The beam waist is defined as the location where the beam radius is at its minimum, and it is influenced by both the focusing characteristics of the optical system and the propagation distance. The non-linear behaviour observed in beam waist across different *iMP* values can be attributed to how Gaussian beams propagate. The paraxial approximation, which is often used to describe Gaussian beams, assumes that the beam diverges slowly and that its waist size is sufficiently large compared to the wavelength. As focusing becomes tighter (especially near or below certain thresholds), this approximation begins to fail, leading to non-linear relationships between parameters like waist size and magnification power. The configuration of lenses and their focal lengths significantly impacts how tightly a beam can be focused and how its waist behaves under varying conditions. When adjusting *iMP*, especially beyond certain points (~66.66%), the system may reach a point where further magnification leads to diminishing returns on focusing capability, hence causing fluctuations in beam waist size. The behaviour of beam waist can also be influenced by physical constraints such as diffraction limits and energy distribution within the beam profile, which may not scale linearly with changes in optical parameters.

4.2 Influence of iMP and c on beam waist, angle of divergence, and beam quality

The M^2 shows an inverted U-shape, decreasing from 43.38 to 29.02 as *iMP* increases from 0% to 100% for a 60 mm achromatic doublet at c = 2 mm, with a maximum value of 49.38 at *iMP* = 33.33% (see Fig. 5). The *BPP* also exhibits an inverted U-shape, changing from 11.16 mm·mrad to 7.46 mm·mrad with *iMP* from 0% to 100%, peaking at 12.7 mm·mrad when *iMP* = 33.33%. θ decreases from 89.27 mrad to 49.75 mrad as *iMP* increases from 0% to 100%. Both M^2 and *BPP* show a non-linear relationship with *iMP*, characterized by maxima at specific points, while θ shows a consistent decreasing trend. The results indicate that as *iMP* increases, both M^2 and *BPP* initially increase (decline in quality) before decreasing (improving), suggesting that there are optimal ranges of magnification where beam quality is whether minimized or maximized. The inverted U-shape behaviour of both the beam quality factor and *BPP* suggests that there are optimal configurations around *iMP* = 0% and *iMP* = 100%, where the focusing conditions are ideal for achieving high-quality beams. Between or beyond these points, changing magnification may lead to increased aberrations or suboptimal focusing conditions that degrade beam quality. The half-angle of divergence decreases significantly with increasing *iMP*, indicating that tighter focusing is achieved relative to the increase in working distance and beam radius expansion at the achromatic doublet level as inverted magnification increases. Since *BPP* is defined as the product of beam waist and half-angle divergence, this relationship explains why *BPP* decreases concurrently with improved focusing conditions at certain magnifications.

The beam quality factor fluctuates from 43.23 to 36.42 to 44.65 to 37.38 as *iMP* varies from 0% to 33.33% to 66.66% to 100% for a 60 mm achromatic doublet at c = 0 mm, indicating variability in beam quality across these magnification settings (see Fig. 6). The *BPP* changes similarly, moving from 11.11 mm·mrad to 9.37 mm·mrad to 11.48 mm·mrad to 9.61 mm·mrad with the same *iMP* variations, suggesting that beam quality is not consistent across all settings. θ decreases consistently from 88.95 mrad to 48.07 mrad as *iMP* increases from 0% to 100%, indicating improved focusing capability at higher magnifications. Both beam quality factor and *BPP* exhibit non-linear behaviour with fluctuations at specific *iMP* values, while θ shows a clear decreasing trend.

The fluctuating nature of both the beam quality factor and *BPP* suggests that there is no single optimal setting for these parameters across the entire range of *iMP* values. Instead, there are specific points where beam quality may be enhanced or degraded. The observed fluctuations in beam quality factor and *BPP* could be attributed to variations in how well the optical system focuses the laser beam at different magnifications. These results indicate that certain configurations may introduce aberrations or other optical effects that impact beam quality. The consistent decrease in θ with increasing *iMP* indicates that tighter focusing is achieved at higher magnifications, which is beneficial for applications requiring precise targeting and ignition.

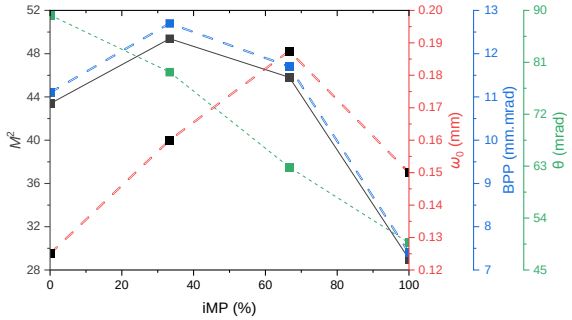

Fig. 5. Variation M^2, ω_0, *BPP*, and θ with *iMP* at c = 2 mm.

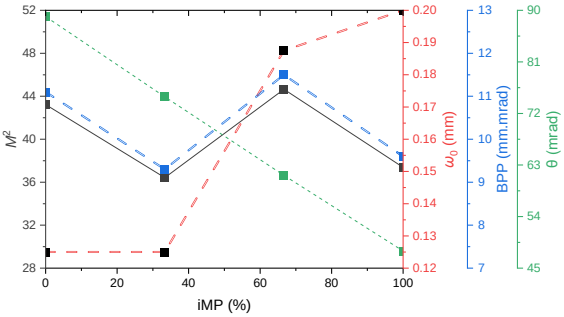

Fig. 6. Variation M^2, ω_0, *BPP*, and θ with *iMP* at c = 0 mm.

To compare the results for the two cases (c = 0 mm and c = 2 mm) with a 60 mm achromatic doublet, and to explain the observed trends in beam quality factor and *BPP*, some considerations are furtherly discussed and analysed. When c = 2 mm, the beam quality factor shows an inverted U-shape, decreasing from 43.38 to 29.02, peaking at 49.38 at *iMP* = 33.33%, then decreasing again. The *BPP* also exhibits an inverted U-shape, changing from 11.16 mm·mrad to 7.46 mm·mrad, peaking at 12.7 mm·mrad at *iMP* = 33.33%. θ decreases from 89.27 mrad to 49.75 mrad with increasing *iMP*. When c = 0 mm, the beam quality factor fluctuates from 43.23 to 36.42 to 44.65 to 37.38 as *iMP* varies from 0% to 33.33% to 66.66% to 100%. The *BPP* changes from 11.11 mm·mrad to 9.37 mm·mrad to 11.48 mm·mrad to 9.61 mm·mrad with the same *iMP* variations. θ decreases from 88.95 mrad to 48.07 mrad as *iMP* increases from 0% to 100%. The beam quality factor and BPP show similar trends in both cases, indicating that changes in magnifying power affect these parameters consistently across different compensator settings. The first case (c = 2 mm) exhibits a more defined inverted U-shape trend, while the second case (c = 0 mm) shows fluctuations in beam quality factor and *BPP*. The reason for both beam quality factor and *BPP* showing similar trends across the two cases is that they are inherently related through their definitions, and as both parameters are influenced by the same optical conditions (i.e., focusing characteristics of the achromatic doublet and adjustments made by the compensator), their trends reflect similar underlying physics. Variations of the trends related to the beam quality factor and *BPP* may arise due to increased sensitivity of the optical setup to alignment or aberrations introduced by lens imperfections at shorter working distances; nevertheless, the lack of a clear peak at some compensator positions may indicate that the system achieves better focusing conditions consistently across the range of *iMP* values. While both cases demonstrating that lower values of beam quality factor and *BPP* indicate better beam quality, their specific behaviours differ due to how compensator position influences optical stability and performance within the setup.

4.3 Effects of input power, beam waist, beam quality, iMP, and c on intensity and brightness

The increase in beam waist from *iMP* = 0% to *iMP* = 66.66% at c = 2 mm and input power of 2W suggests that the beam is becoming less focused, which correlates with the observed decrease in intensity during this range, from 1820 W/cm^2 to 995 W/cm^2 (see Fig. 7). The decrease in beam waist at *iMP* = 100% indicates a return to tighter focusing conditions, which may contribute to the increase in intensity observed, reaching 1650 W/cm^2. The consistent decrease in half angle of divergence with increasing *iMP* indicates that higher inverted magnification leads to better collimation of the beam, reducing divergence and improving focusability. The findings suggest an optimal range for *iMP* settings that balances beam focus and intensity without entering regions of increased divergence or saturation.

The increase in laser intensity from *iMP* = 0% to *iMP* = 33.33% at c = 0 mm and input power of 2W suggests that the beam is becoming more effectively focused while the beam waist remained unchanged and the half angle of divergence decreased, resulting in higher energy concentration on the target area (see Fig. 8).

The subsequent decrease in intensity at *iMP* values of 66.66% and then at 100% indicates that further inverted magnification leads to adverse effects on beam quality and focusability, due to increased beam waist. The beam waist remains constant at 0.125 mm for both *iMP* values of 0% and 33.33%. However, it increases significantly at higher inverted magnifications (to 0.1875 mm at *iMP* = 66.66% and further to 0.2 mm at *iMP* = 100%). This trend suggests that as inverted magnification increases, the effective focus diminishes, which correlates with the observed drop in intensity. The consistent decrease in half angle of divergence from approximately 88.95 mrad to about 48.07 mrad as *iMP* increases indicates that higher inverted magnification leads to better collimation of the beam, reducing divergence. These trends support the idea that while increasing inverted magnification can initially improve focus, there is an optimal range beyond which further inverted magnification leads to adverse effects on intensity and beam quality. The variation in laser brightness is inversely proportional to the variation in M^2 and *BPP*. When the latter increase (poorer beam quality), the former decreases, and vice-versa, when the latter decrease (better beam quality), the former increases (see Fig. 9 and Fig. 10).

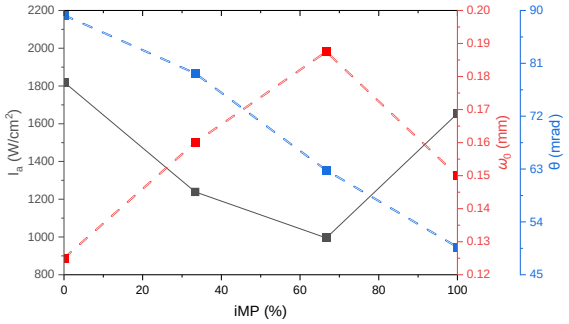

Fig. 7. Variation of I_a, ω_0, and θ with *iMP* at c = 2 mm.

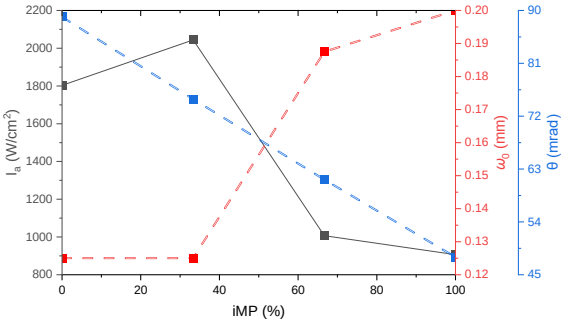

Fig. 8. Variation of I_a, ω_0, and θ with *iMP* at c = 0 mm.

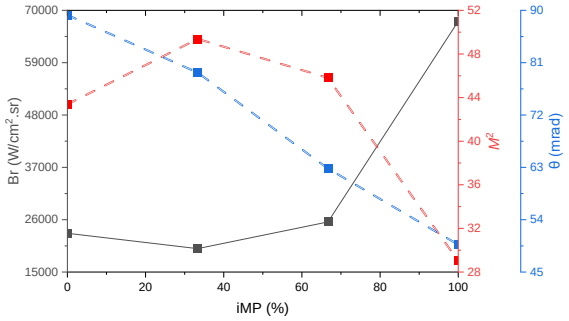

Fig. 9. Variation of laser brightness, M^2, and θ with *iMP* at c = 2 mm.

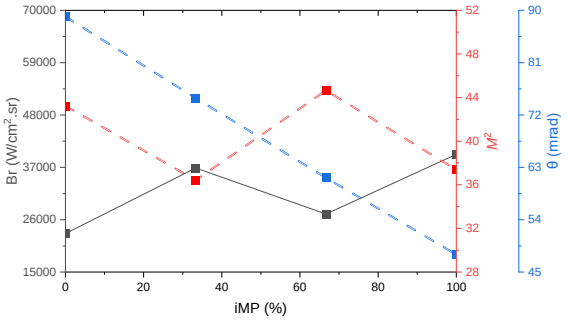

Fig. 10. Variation of laser brightness, M^2, and θ with *iMP* at c = 0 mm.

4.4 Effects of beam waist and laser brightness on laser intensity

The incident intensity increases proportionally with input power across both beam waist configurations. The increase rate of incident intensity is higher when the beam waist is set to 0.125 mm compared to 0.1875 mm, indicating that a smaller beam waist leads to greater intensity for the same input power. Notably, the increase rate of incident intensity diminishes when input power is 1.5W and 2W for both beam waists, suggesting saturation effects. As the input power approaches certain thresholds, the gain medium may not be able to efficiently convert all input energy into increased output intensity due to limitations such as thermal effects or saturation of excited states. The proportional increase in incident intensity with input power aligns with the expected behaviour of laser systems where higher input power results in greater energy concentration. The higher increase rate observed with a smaller beam waist (0.125 mm) can be attributed to increased intensity due to tighter focusing.

Another observation needs to be analysed regarding incident intensity under different configurations of *iMP* and c but with similar beam waists. The intensity is similar for configurations where the beam waist is 0.125 mm, specifically for c = 0 mm and *iMP* = 0% ($d_{working}$ = 75 mm), and c = 2 mm and *iMP* = 0% ($d_{working}$ = 70 mm). However, the intensity is significantly higher when c = 0 mm and *iMP* = 33.33% ($d_{working}$ = 100 mm) compared to other configurations. The beam waist of 0.125 mm indicates that all configurations are designed to focus the laser beam effectively.

Even with identical beam waists, variations in working distance and optical path length can affect how intensity is distributed. The optical path length changes with different *iMP* and *c* settings. A shorter path may allow less divergence and better energy concentration at the target area. The divergence of the beam is inversely related to the beam waist; thus, a smaller waist at optimal focusing conditions can lead to greater intensity despite similar waist sizes across different configurations. Another reason is that both beam quality factor and *BPP* are smaller (high beam quality) for c = 0 mm and *iMP* = 33.33% ($d_{working}$ = 100 mm) compared to the other configurations. Therefore, higher beam quality leads to higher laser brightness. This is also true for c = 0 mm and *iMP* = 0% ($d_{working}$ = 75 mm), and c = 2 mm and *iMP* = 0% ($d_{working}$ = 70 mm) as these both configurations have similar but high beam quality factors and *BPP*, leading to lower beam quality, as shown previously. The same can be said for the configurations c = 0 mm and *iMP* = 66.66% ($d_{working}$ = 140 mm), and c = 2 mm and *iMP* = 66.66% ($d_{working}$ = 115 mm), but with similar beam quality factors and nearly identical incident intensities focused over equal areas with same beam waists (see Fig. 11 and Fig. 12).

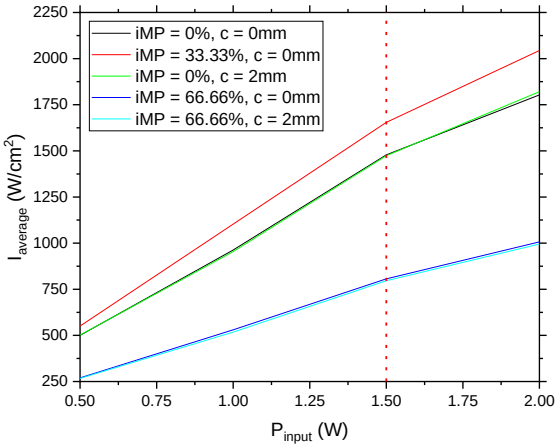

Fig. 11. Variation of incident intensity with P_{input} using different configurations.

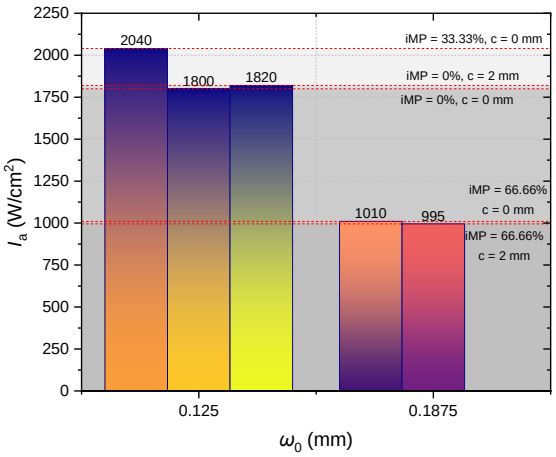

Fig. 12. Variation of incident intensity with ω_0 using different configurations at P_{input} = 2W.

4.5 Energy input and 60-mm configuration effects on ignition delay time

An initial set of experiments utilized a 60-mm achromatic doublet, with the parameters iMP and c configured at 0% and 2 mm, respectively. A 0.125-mm beam waist was obtained at the focal point with a 70-mm working distance. For each new configuration, input power was varied in a descending manner from 2 W to 0.5 W in increments of 0.5 W, and pulse durations were systematically readjusted to their minimum values required to deliver sufficient pulse energy for ignition to occur. The results indicated that at an input power of 2 W, the required pulse duration was 50 ms, resulting in an ignition delay time of 20 ms. At an input power of 1 W, the necessary pulse duration increased to 100 ms, with an ignition delay time of 30 ms. At the lowest tested input power of 0.5 W, the required pulse duration further increased to 630 ms, accompanied by an ignition delay time of 500 ms. These findings demonstrate a clear sensitivity of the ignition process to variations in laser power (see Fig. 13).

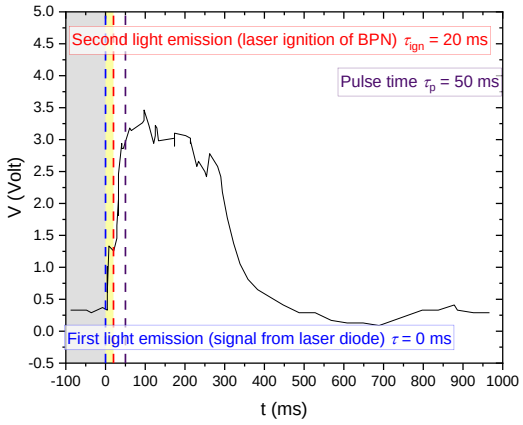

(a) P_{input} = 2000 mW, t_p = 50 ms

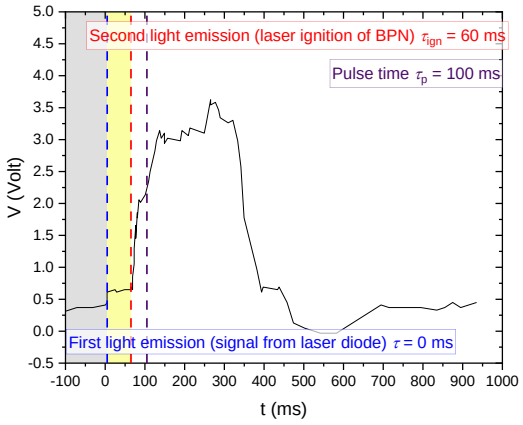

(b) P_{input} = 1500 mW, t_p = 100 ms

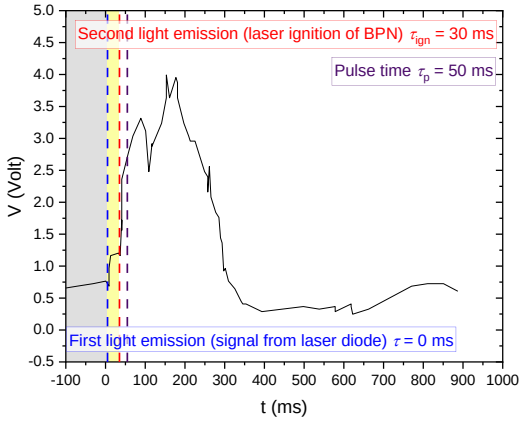

(c) P_{input} = 1250 mW, t_p = 50 ms

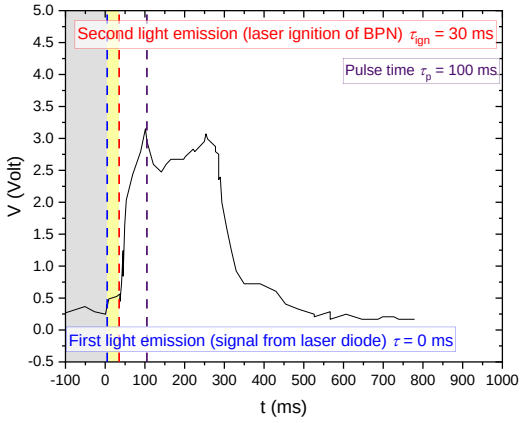

(d) P_{input} = 1000 mW, t_p = 100 ms

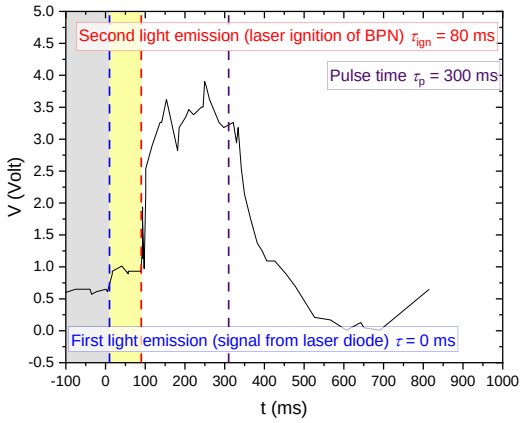

(e) P_{input} = 875mW, t_p = 300ms

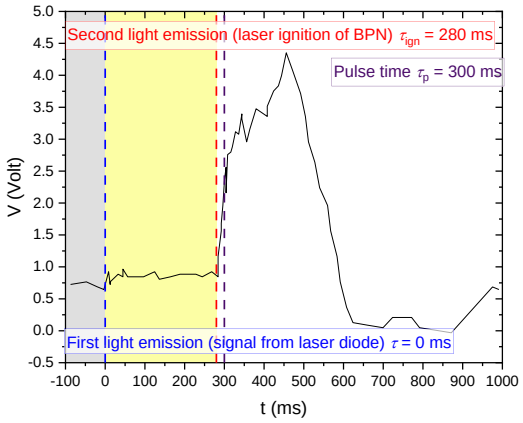

(f) P_{input} = 750mW, t_p = 300ms

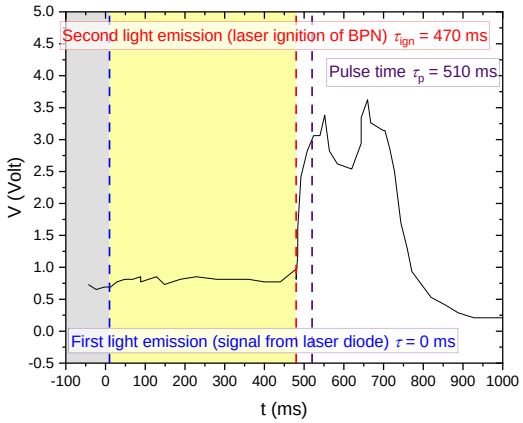

(g) P_{input} = 600mW, t_p = 510ms

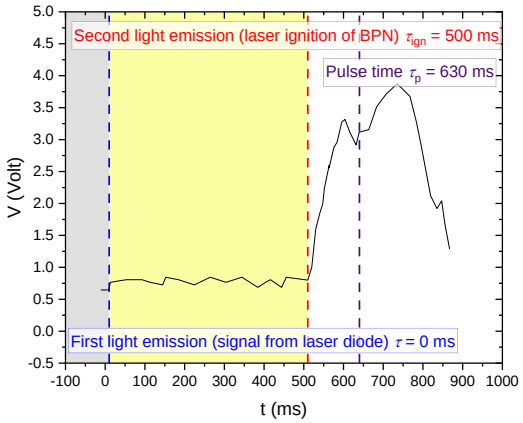

(h) P_{input} = 500mW, t_p = 630ms

Fig. 13 Variation of ignition delay with P_{input} and t_p at c = 2 mm, iMP = 0%, f_{dblt} = 60 mm.

Another set of experiments utilized a 60-mm achromatic doublet, with the parameters for iMP and c configured at 100% and 2 mm, respectively, and a 0.15-mm beam wait was obtained at the focal point with a 170-mm working distance. The same protocol was adopted for each configuration. The results indicated that at an input power of 2 W, the required pulse duration was 50 ms, resulting in an ignition delay time of 20 ms. At an input power of 1.5 W, the necessary pulse duration increased to 60 ms, with an ignition delay time of 60 ms. At an input power of 1 W, the necessary pulse duration increased to 110 ms, with an ignition delay time of 70 ms. At an input power of 0.9 W, the required pulse duration further increased to 110 ms, accompanied by an ignition delay time of 110 ms. At an input power of 0.75 W, the required pulse duration further increased to 400 ms, accompanied by an ignition delay time of 210 ms. At the lowest input power of 0.6 W, the required pulse duration further increased to 500 ms, accompanied by an ignition delay time of 420 ms (see Fig. 14).

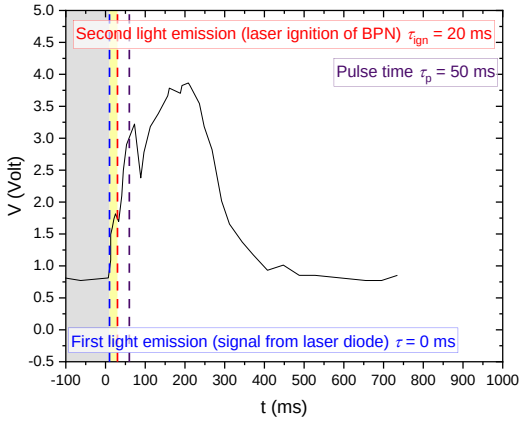

(a) P_{input} = 2000mW, t_p = 50ms

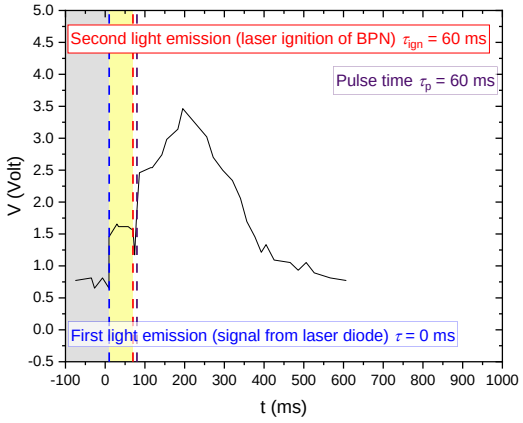

(b) P_{input} = 1500mW, t_p = 60ms

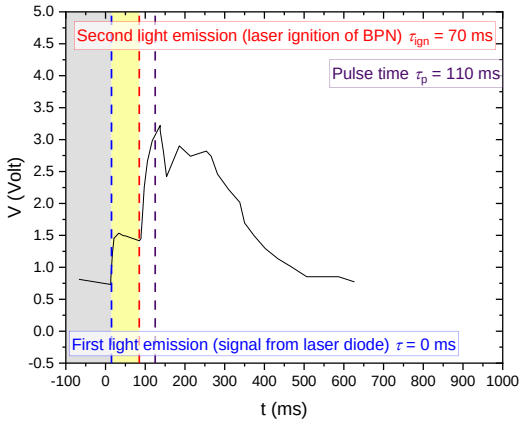

(c) P_{input} = 1000mW, t_p = 110ms

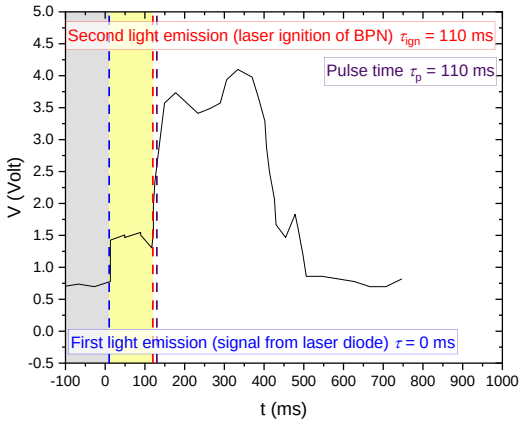

(d) P_{input} = 900mW, t_p = 110ms

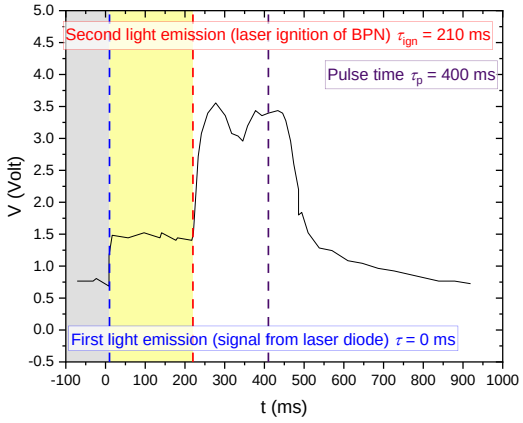

(e) P_{input} = 750mW, t_p = 400ms

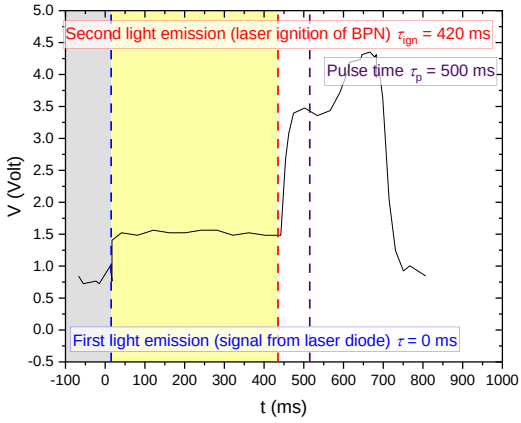

(f) P_{input} = 600mW, t_p = 500ms

Fig. 14. Variation of ignition delay with P_{input} and t_p at c = 2 mm, iMP = 100%, f_{dblt} = 60 mm.

The comparison between setups indicates that while higher power levels lead to faster ignition, the transition from one power level to another is not uniform across configurations. A broader focus may influence energy distribution. The increase in working distance could lead to reduced intensity at the sample due to beam divergence over a longer distance. However, if the M² value decreases, it indicates an improvement in beam quality despite the broader beam waist, which may enhance energy delivery efficiency. The results indicate that increasing iMP leads to varied responses in terms of pulse time and ignition delay, suggesting that laser energy distribution and focus play critical roles in ignition efficiency. The significant increase in pulse times at lower power levels (e.g., from 1W to 0.75W) suggests that BPN exhibits a threshold behaviour where reduced energy input drastically affects the ignition process. The change in optical parameters (beam waist, working distance, and M²) indicates that careful optimization of these factors is essential for achieving effective ignition, particularly when working with different configurations.

5. Conclusions

The findings highlight the intricate nature of optimizing laser systems for practical applications, which are not only limited to laser ignition. Future research will utilize these insights to enhance optical system designs that are crucial for investigating the laser-matter interactions and their relevant characteristics. These results have facilitated the development of tailored laser configurations, primary energetic materials selection, and laser ignition systems combination processes. Additionally, the significance of precise thermal management and identified potential strategies were underscored for improving efficiency through the strategic selection of optical laser parameters, energy-related performance metrics, and material characteristics. Actual laser beams often exhibit deviations from the ideal behaviour. To quantify these deviations, the beam quality factor (M^2) and the beam parameter product (BPP) were introduced, allowing for a comparison between the performance of real laser beams and diffraction-limited Gaussian beams.

Essential parameters such as beam radius, intensity distribution, and laser brightness were derived from the governing equations such as Helmholtz's, Maxwell's, paraxial wave's, and Gaussian distribution equations, supported by experimental data. The relationship between optical (geometric) beam parameters was furtherly explored through measurements and comparisons, providing insights into the practical implications of these metrics and configurations in laser ignition applications. The analysis of dynamic optical system configurations for beam propagation revealed key differences between fixed and variable optical systems. Fixed optical systems are valued for their simplicity and stability, ensuring reproducibility. However, their lack of adaptability restricts their use in dynamic environments. In contrast, dynamic optical configurations provide greater flexibility in accordance to the requirements.

In this research, several optical configurations and performance metrics were introduced. The results indicated that there is no single optimal setting for M^2 and *BPP*; however, specific points exist where these parameters can improve or degrade under specific conditions. The differences in behaviour between configurations highlight how inverted magnifications (*iMP*) and compensator positions (*c*) affect optical stability and performance. Also, the interplay of input power, pulse time, *iMP*, and c significantly affects pulse energy, intensity distribution, and laser brightness dynamics. Differences in optical path length and dispersion between compensator positions can affect how energy accumulates over time. Variations in laser intensity occur among different configurations with similar beam waists. For instance, configurations with a beam waist of 0.125 mm show similar intensities for c = 0 mm and *iMP* = 0% compared to c = 2 mm and *iMP* = 0%, but a higher intensity is achieved at c = 0 mm and *iMP* = 33.33% due to higher brightness at this specific optical configuration when compared to the two previous ones. This indicates that in addition to the effective focal length and optical path length, laser brightness also significantly influences laser intensity. The variation in laser brightness is inversely related to changes in M^2 and *BPP*. As beam quality decreases (indicated by higher M^2 and *BPP* values), laser brightness also declines, and vice versa. These findings highlight the importance of optimizing *iMP* and *c* settings to enhance laser brightness while maintaining effective beam quality across different input power levels, pulse times, and effective focal lengths.

The interaction between laser light and Boron Potassium Nitrate (BPN) is a complex process influenced by the intrinsic properties of BPN and the parameters of the laser used. The dynamics of thermal interactions in BPN are primarily governed by principles of heat transfer. Ignition dynamics of BPN are sensitive not only to variations in energy-related parameter metrics, but also to optical (geometric) beam parameters. For instance, using a 60-mm converging achromatic doublet with an effective focal length of 70 mm (ω_0 = 0.125 mm, *iMP* = 0%, and c = 2 mm), a 2-W input power and a 50-ms pulse time resulted in a 20-ms ignition delay time. Similarly, if the beam waist is kept relatively small (ω_0 = 0.125 mm) in relation to the beam radius, angle of divergence, and overall beam quality, then whether using a 60-mm or a 125-mm converging achromatic doublet at longer effective focal lengths of 170 mm (*iMP* = 100% and c = 2 mm), 190 mm (*iMP* = 0% and c = 2 mm), respectively, or larger, this still provided ignition delay times of 20 ms for each of these configurations.

In contrast, non-optimal configurations exhibited longer ignition delay times, sometimes exceeding 400 ms. Conversely, lower power levels necessitated longer pulses to achieve ignition. Also, experiments with varying *iMP* and *c* settings revealed that larger beam waists decrease energy concentration, requiring extended pulse durations for successful ignition. Beam waists significantly influences surface temperature during ignition. High input power favoured diffusive heat transfer for immediate ignition, while lower powers allowed both diffusive and convective mechanisms, leading to longer pulse and ignition delay times. Another finding from this research is the relationship between the beam waist and threshold ignition power (instantaneous power level to be applied to achieve ignition). Increasing the beam waist from 0.125 mm to 0.1875 mm raised the threshold ignition power due to reduced energy concentration at the surface. An inversely proportional relationship was observed between threshold ignition energy (minimum amount of energy delivered over a specific period to achieve ignition) and threshold ignition power. Different configurations affected energy requirements; for instance, less energy was needed when c = 0 mm compared to c = 2 mm. It is essential to recognize how these findings not only advance the understanding of laser ignition dynamics but also introduce innovative approaches to optimizing laser systems. The insights gained from this research pave the way for new methodologies in tailoring laser configurations and enhancing laser-materials interactions.

Acknowledgements

The authors would like to thank the institutions and personnel who actively contributed and supported this research by providing the facilities and resources necessary for the successful completion of this work.

References

[1] J. van der Geer, J.A.J. Hanraads, R.A. Lupton, The art of writing a scientific article, J. Sci. Commun. 163 (2010) 51–59.
[2] J. Wang, Y. Li, J. Zhang, et al., Industrial Applications of Laser Technology in Manufacturing, J. Laser Appl. 34 (2016) 321-332.
[3] M. D. Smith, D.A. Jackson, Spectroscopy and Holography with Lasers, J. Appl. Opt. 42 (2014) 4235-4241.
[4] H. Zhou, W. Zhang, P. Chen, Holographic Optical Tweezers in Cell Manipulation, J. Opt. Lett. 35 (2015) 2483-2485.
[5] C. T. Liao, H. Zhang, R. C. Xu, Fiber-optic Communication Systems and Lasers, J. Opt. Comm. 42 (2017) 345-351.
[6] F. R. Ortiz, K. Krug, Laser Weapons in Modern Military Applications, J. Military Sci. 56 (2019) 72-80.
[7] M. K. Gupta, N. R. Mishra, Laser Ignition of Energetic Materials, J. Propellants Explos. Pyrotech. 42 (2017) 220-231.
[8] A. V. Gotsky, R. B. Regan, J. F. Smith, Safety and Control in Laser Ignition of Explosives for Aerospace Applications, J. Eng. Safety 31 (2020) 112-120.
[9] L. X. Liu, Z. B. Wang, Selection of Boron Potassium Nitrate for Laser Ignition, J. Combust. Sci. Tech. 31 (2018) 90-98.
[10] J. N. Miller, T. A. Garcia, The Role of BPN in Laser Ignition Systems, J. Chem. Eng. 45 (2021) 34-41.
[11] R. G. Menke, A. S. Lee, Optimization of Beam Delivery Systems for Laser Ignition, J. Appl. Opt. 55 (2018) 1350-1357.
[12] P. H. Lee, J. D. Wang, Beam Divergence and Alignment Challenges in Laser Propagation, J. Opt. Commun. 44 (2019) 1110-1115.
[13] D. L. Arnold, G. B. Roberts, Energy Conservation in Laser Systems for Propellant Ignition, J. Laser Phys. Lett. 32 (2020) 1117-1122.
[14] F. A. Peters, L. W. Howell, Optimization of Laser Parameters for Enhanced Material Interaction, J. Laser Sci. Tech. 40 (2018) 82-90.
[15] B. C. Smith, J. W. Hines, Laser Ignition: Effect of Focal Lengths and Working Distances, J. Appl. Laser Phys. 60 (2021) 107-114.